PHYSICAL REVIEW D **95,** 036018 (2017)

Electrical conductivity of hadronic matter from different possible mesonic and baryonic loops

Sabyasachi Ghosh*

Department of Physics, University of Calcutta, 92, A. P. C. Road, Kolkata 700009, India

(Received 6 July 2016; published 22 February 2017)

Electromagnetic current-current correlators in pionic and nucleonic medium have been evaluated in the static limit to obtain electrical conductivities for pion and nucleon components, respectively, where the former decreases and the latter increases with the variation of temperature T and baryon chemical potential μ_N. Therefore, total electrical conductivity of pion and nucleon system exhibits a valley structure in the T-μ_N plane. To get nondivergent and finite values of correlators, and finite thermal widths of medium constituents, the pion and nucleon have been considered, where the thermal widths have been determined from the in-medium scattering probabilities of the pion and nucleon with other mesonic and baryonic resonances, based on the effective hadronic model. At $\mu_N = 0$, the results of the present work more or less agree with the results of earlier works and their finite μ_N extension shows a decreasing nature of electrical conductivity for the hadronic medium.

DOI: 10.1103/PhysRevD.95.036018

I. INTRODUCTION

The electromagnetic current-current correlator at finite temperature is one of the very important quantities to characterize the medium, produced in high energy heavy ion collisions. The explicit dynamical structure of this quantity for hadronic matter (HM) is directly linked with the in-medium spectral functions of neutral vector mesons and also with the thermal dilepton and photon yields from HM, whereas its static limit provides the estimation of an important transport coefficient like electrical conductivity (σ) of the HM. According to recent reviews [1,2], the effective field theoretical calculations of hadrons at finite temperature are very successful in describing the low mass dimuon enhancement measured by the NA60 Collaboration [3]. This low mass enhancement also gets a boost from the quark matter sources, which have been calculated by using the hard thermal loop technique in Ref. [4] (see also Ref. [5] for effective QCD model calculation). Therefore, it is very interesting and phenomenologically important to know the static limit estimation of the dynamical structure of the current-current correlator by calculating σ of the hadronic medium in the framework of the effective hadronic model. This is basically attempted by this present work.

The event by event analysis [6] in relativistic heavy ion collisions indicates the possibility of generation of high strength electric (E) and magnetic (B) fields in the medium. For example, in the relativistic heavy ion collider (RHIC) experiment, their approximate values are $eB \approx m_\pi^2 \approx 10^{18} G$ and $eE \approx m_\pi^2 \approx 10^{21} V/cm$ [7], although a particular magnetic field component only becomes nonzero in the average scenario [6,7]. The time evolution of this average magnetic field [7] depends on the σ of the expanding medium, produced in heavy ion collisions, which demands that we have some good idea of the numerical value of this σ.

In Ref. [8], the electrical conductivity or the electric charge diffusion coefficient of the evolving medium is used as input to explain the low mass dilepton enhancement, observed experimentally by the PHENIX Collaboration at the RHIC; whereas, Yin [9] has shown that the electrical conductivity of quark-gluon plasma (QGP) plays an important role to regulate the soft photon production via realistic hydrodynamics simulation. Besides these indirect estimations of electrical conductivity of QGP, it can directly be extracted from charge dependent direct flow parameters in asymmetric heavy ion (Au + Cu) collisions [10]. Along with these phenomenological studies, different microscopic calculations for σ of the quark [11–17] and hadronic phase [18–21] have been done, although the results of Cassing *et al.* [11] in the model of parton hadron string dynamics (PHSD) and the Nambu-Jona-Lasino (NJL) model results of Marty *et al.* [12] have covered σ estimation for the temperature domain of both quark and hadronic matter. On this problem, a large number of lattice QCD calculations have been done [22–28], where their estimations cover a large numerical band (see Table I, addressed in the results section). Now, from the calculations [18–21] in the hadronic temperature domain, we see that the results of Refs. [18] and [19–21] show a completely opposite nature of temperature (T) dependence of σ. If we considered the results of Lee *et al.* [18] as an exception, almost all of the earlier works [11–17,19–21,28] indicate that σ/T decreases in the hadronic temperature domain [11,12,19–21] and increases in the temperature domain of the quark phase [11–17,28]. Their numerical values are located within the

*sabyaphy@gmail.com

TABLE I. At $\mu_N = 0$, the $\sigma(T)/T$ in the approximated temperature domain of hadronic ($T \approx 0.120$ GeV to 0.175 GeV) and quark ($T \approx 0.175$ GeV to 0.350 GeV) phases are presented in the second and third columns, whereas in the first column, the references (with their methodologies) are addressed.

	σ/T at $T = (0.120$–$0.175)$ GeV	σ/T at $T = (0.175$–$350)$ GeV
LQCD Results:		
Gupta [26]	⋯	≈ 0.375
Ding *et al.* [22]	⋯	$\approx 0.033(+0.018, -0.016)$
Arts *et al.* [23]	⋯	$\approx 0.020(\pm 0.005)$
Brandt *et al.* [27]	⋯	$\approx 0.020(\pm 0.006)$
Burnier *et al.* [25]	⋯	≈ 0.0064
Amato *et al.* [28]	⋯	$\approx 0.003(\pm 0.001)$ -0.015($\pm$0.003)
Buividovich *et al.* [24]	⋯	$\approx 0.0021(\pm 0.0003)$
Yin [9]	⋯	$\approx 0.06(+0.04, -0.02)$
Puglisi *et al.* [13] (PQCD in RTA)	⋯	$\approx 0.09 - 0.13$
Puglisi *et al.* [13] (QP in RTA)	⋯	$\approx 0.01 - 0.07$
Greif *et al.* [14] (BAMPS)	⋯	$\approx 0.04 - 0.06$
Marty *et al.* [12] (DQPM)	⋯	$\approx 0.06 - 0.16$
Marty *et al.* [12] (NJL)	$\approx 0.06 - 0.05$	$\approx 0.05 - 0.5$
Cassing *et al.* [11] (PHSD)	$\approx 0.088 - 0.025$	$\approx 0.025 - 0.2$
Finazzo *et al.* [16]	$\approx 0.004 - 0.010$	$\approx 0.010 - 0.015$
Lee *et al.* [18]	$\approx 0.001 - 0.011$	$\approx 0.36 - 0.015$
Fraile *et al.* [20] (unitarization)	$\approx 0.013 - 0.010$	⋯
Fraile *et al.* [20] (ChPT)	$\approx 0.008 - 0.002$	⋯
Present results	$\approx 0.004 - 0.001$	⋯

order $\sigma/T \approx 10^{-3}$ to 10^{-2} for the hadronic phase and $\sigma/T \approx 10^{-3}$ to 10^{-1} for the quark phase. This information from earlier studies indicates that the numerical strength as well as the nature of $\sigma(T)$ has not been a a very settled issue until now.

In this context, the present investigation is a similar kind of microscopic calculation for σ of hadronic matter, which is expected to update our understanding of $\sigma(T)$ and converge towards a settled direction. Considering the pion and nucleon as abundant constituents of hadronic matter, we have calculated their electromagnetic current-current correlators at finite temperature, whose static limits give the estimation of σ for the respective components. As an interaction part, the effective hadronic Lagrangian densities have been used to calculate the in-medium scattering probabilities of the pion and nucleon with other mesonic and baryonic resonances present in the hadronic medium. Extending our investigations for finite nucleon or baryon chemical potential μ_N, the present results provide the estimation of σ in the T-μ_N domain of hadronic matter.

The basic formalism of σ is addressed in Sec. II, where we see that the nondivergent values of respective current-current correlators are mainly regulated by the thermal widths of medium components, which are calculated and briefly described in Sec. III. Calculations of different loop diagrams are classified in three subsections. After it, the numerical discussions have been addressed in Sec. IV, which is followed by a discussion of higher order issues in Sec. V and at last, the studies are summarized in Sec. VI.

II. FORMALISM OF ELECTRICAL CONDUCTIVITY

Owing to the famous Kubo formula [29,30], the electrical conductivity in momentum space can be expressed in terms of spectral density of the current-current correlator as [20]

$$\sigma = \frac{1}{6} \lim_{q_0, \vec{q} \to 0} \frac{A_\sigma(q_0, \vec{q})}{q_0}, \tag{1}$$

where $A_\sigma(q_0, \vec{q}) = \int d^4x e^{iq\cdot x} \langle [J_i^{\rm EM}(x), J^i_{\rm EM}(0)] \rangle_\beta$, $\langle .. \rangle_\beta$ denotes the thermodynamical ensemble average and $J_\mu^{\rm EM}(x))$ is the electromagnetic current.

In real-time thermal field theory (RTF), any two point function at finite temperature always has a 2×2 matrix structure. Hence, the thermal correlator of the electromagnetic current can be expressed as

$$\Pi^{ab}(q) = i \int d^4x e^{iqx} \langle T_c J_\mu^{\rm EM}(x) J^\mu_{\rm EM}(0) \rangle^{ab}_\beta, \tag{2}$$

where T_c denotes the time ordering with respect to a symmetric contour in the complex time plane. For this contour, we get four possible sets of two points and therefore, we get 2×2 matrix structure of the two point function. The superscripts $a, b (= 1, 2)$ in Eq. (2) represent the (thermal) indices of the matrix. The retarded part of the correlator $\Pi^R(q)$ and its corresponding spectral density $A_\sigma(q)$ can be extracted from 11-component $\Pi^{11}(q)$ by using the relation

$$A_\sigma(q) = 2{\rm Im}\Pi^R(q) = 2 \tanh\left(\frac{\beta q_0}{2}\right) {\rm Im}\Pi_{11}(q). \tag{3}$$

Using this relation (3), Eq. (1) can alternatively be expressed as

$$\begin{aligned} \sigma &= \frac{1}{3} \lim_{q_0, \vec{q} \to 0} \frac{{\rm Im}\Pi^R(q_0, \vec{q})}{q_0} \\ &= \frac{1}{3} \lim_{q_0, \vec{q} \to 0} \frac{\tanh(\frac{\beta q_0}{2}) {\rm Im}\Pi^{11}(q_0, \vec{q})}{q_0}. \end{aligned} \tag{4}$$

Since pion and nucleon constituents are our matter of interest, we should focus on their electromagnetic currents,

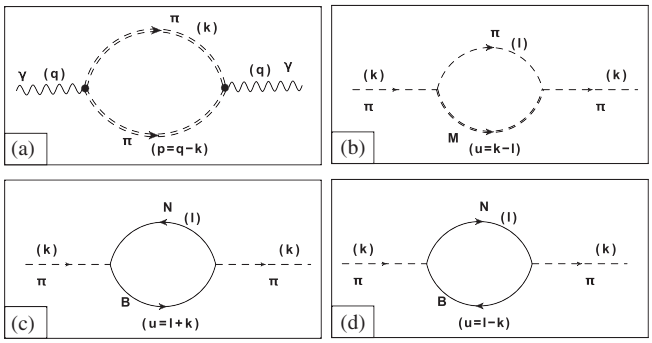

FIG. 1. The diagram (a) is a schematic one-loop representation of the electromagnetic current-current correlator for the medium with pionic constituents. The external photon lines are coupled with double dashed internal lines of pions, which have some finite thermal width. The thermal width of the pion can be derived from its self-energy diagrams (b)–(d), where (b) represents pion self-energy for mesonic (πM) loops, whereas diagrams (c) and (d) are direct cross diagrams of pion self-energy for NB loops.

$$J^{\mu}_{\pi} = e\phi_{\pi}(\partial^{\mu}\phi_{\pi}) \quad \text{and} \quad J^{\mu}_{N} = e\overline{\psi}_{N}\gamma^{\mu}\psi_{N}, \tag{5}$$

which are electromagnetically coupled with the photon via interaction (QED) Lagrangian density

$$\mathcal{L} = -(J^{\mu}_{\pi} + J^{\mu}_{N})A_{\mu}. \tag{6}$$

Since (ϕ_{π^+}, ϕ_{π^-}) from the pion triplet (ϕ_{π^+}, ϕ_{π^-}, ϕ_{π^0}) and the proton (ψ_p) from the nucleon doublet (ψ_p, ψ_n) have nonzero electric charges, we have to keep in mind the relevant isospin factors $I^e_{\pi} = 2$ and $I^e_N = 1$, which should be multiplied during our calculations.

To calculate electrical conductivity of the pionic (σ_{π}) and nucleonic (σ_N) medium from their corresponding spectral densities or the retarded part of the correlator via Eq. (4), let us start from the 11 component of the Π_{ab} matrix. The Wick contraction (see the Appendix) of the pion (ϕ_{π}) and nucleon (ψ_N) fields gives one-loop diagrams of photon self-energy, which are shown in Figs. 1(a) and 2(a), respectively. A general mathematical expression of these diagrams is

$$\Pi^{11}(q) = ie^2 \int \frac{d^4k}{(2\pi)^4} N D^{11}(k) D^{11}(p), \tag{7}$$

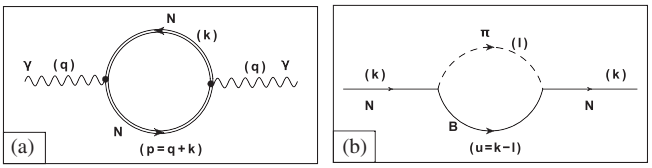

FIG. 2. The diagram (a) is a schematic one-loop representation of the electromagnetic current-current correlator for the medium with nucleonic constituents. Similar to the double dashed lines of pions in Fig. (1), here double solid lines of the nucleon indicate that they have finite thermal width, which can be obtained from the nucleon self-energy diagram (b) for πB loops.

where $D^{11}(k)$ and $D^{11}(p)$ are the scalar parts of propagators, appearing in RTF for the 11 component: $p = q - k$ for the $\pi\pi$ loop in Fig. 1(a), and $p = q + k$ for the NN loop in Fig. 2(a). Multiplication of the vertex part and numerator part of two propagators builds the term N.

In RTF, a general form of $D^{11}(k)$ for the boson or fermion is

$$D^{11}(k) = \frac{-1}{k_0^2 - \omega_k^2 + i\epsilon} + 2\pi i\epsilon_k F_k(k_0)\delta(k_0^2 - \omega_k^2),$$
$$\text{with} \quad F_k(k_0) = n_k^{+}\theta(k_0) + n_k^{-}\theta(-k_0), \tag{8}$$

where $n_k^{\pm}(\omega_k) = \frac{1}{e^{\beta(\omega_k \mp \mu)} - \epsilon_k}$ are the thermal distribution functions and the $\pm$ sign in the superscript of n_k stands for particle and antiparticle, respectively. Now, when we proceed for special cases, pion (boson) or nucleon (fermion) field, we have to put

$$\epsilon_k = +1, \mu = \mu_{\pi} = 0 \text{i.e.} n_k^{+} = n_k^{-},$$
$$\omega_k = \omega_k^{\pi} = (\vec{k}^2 + m_{\pi}^2)^{1/2} \quad \text{for pion}, \tag{9}$$

$$\epsilon_k = -1, \mu = \mu_N (\text{nucleon chemical potential}),$$
$$\omega_k = \omega_k^{N} = (\vec{k}^2 + m_N^2)^{1/2} \quad \text{for nucleon}. \tag{10}$$

However, for the time being we continue our calculation with the general form of D^{11} from Eq. (8) and at a latter stage, we put these conditions (9) and (10) in the general expression.

After using (8) in Eq. (7), if we do its k_0 integration and put it in Eq. (3), then we get spectral density of the electromagnetic current-current correlator [31],

$$A_{\sigma}(q) = e^2 \int \frac{d^3k}{(2\pi)^3} \frac{(-\pi)N}{4\omega_k\omega_p} [C_1\delta(q_0 - \omega_k - \omega_p) + C_2\delta(q_0 - \omega_k + \omega_p) + C_3\delta(q_0 + \omega_k - \omega_p) + C_4\delta(q_0 + \omega_k + \omega_p)], \tag{11}$$

where $\omega_p = \omega_p^{\pi} = \{(\vec{q} - \vec{k})^2 + m_{\pi}^2\}^{1/2}$ for the pion field, and $\omega_p = \omega_p^{N} = \{(\vec{q} + \vec{k})^2 + m_N^2\}^{1/2}$ for the nucleon field. Here N are space components of $N(q, k_0 = \pm\omega_k, \vec{k})$ (see the Appendix),

$$N = (-4)\{-\vec{k}\cdot\vec{q} + \vec{k}^2\} \quad \text{for } \pi\pi\text{loop}, \tag{12}$$

and

$$N = (-8)\{\vec{k}\cdot\vec{q} + \vec{k}^2\} + 4\vec{k}\cdot\vec{q} \quad \text{for } NN\text{loop}. \tag{13}$$

The statistical probabilities, attached with four different delta functions, are

$$C_1 = 1 + n_k^+(\omega_k) + n_p^+(q_0 - \omega_k),$$
$$C_2 = -n_k^+(\omega_k) + n_p^-(-q_0 + \omega_k),$$
$$C_3 = n_k^-(\omega_k) - n_p^+(q_0 + \omega_k),$$
$$C_4 = -1 - n_k^-(\omega_k) - n_p^-(-q_0 - \omega_k), \quad \text{for } \pi\pi\text{loop}; \tag{14}$$

and

$$C_1 = -1 + n_k^-(\omega_k) + n_p^+(q_0 + \omega_k),$$
$$C_2 = -n_k^-(\omega_k) + n_p^-(-q_0 + \omega_k),$$
$$C_3 = n_k^+(\omega_k) - n_p^+(q_0 + \omega_k),$$
$$C_4 = 1 - n_k^+(\omega_k) - n_p^-(-q_0 - \omega_k), \quad \text{for } NN\text{loop}. \tag{15}$$

Four different delta functions are responsible for creating four different regions of branch cuts in the q_0-axis, where $A_\sigma(q_0, \vec{q})$ or $\mathrm{Im}\Pi^R(q_0, \vec{q})$ becomes nonzero. These regions are

$$\begin{aligned} q_0 &= -\infty \text{to} -\{\vec{q}^2 + 4m_{\pi,N}^2\}^{1/2}: \text{ unitary cut,} \\ &= \left.\begin{matrix} -|\vec{q}| & \text{to} & 0 \\ 0 & \text{to} & |\vec{q}| \end{matrix}\right\}: \text{ Landau cut,} \\ &= \{\vec{q}^2 + 4m_{\pi,N}^2\}^{1/2} \text{to} \infty : \text{unitary cut.} \end{aligned} \tag{16}$$

Since electrical conductivity σ is the limiting value of $A_\sigma(q_0, \vec{q})$ or $\mathrm{Im}\Pi^R(q_0, \vec{q})$ at $q_0, \vec{q} \to 0$, we should focus on Landau cuts only. Hence, using the Landau part of Eq. (11) in Eq. (1), we have

$$\begin{aligned} \sigma &= \frac{e^2}{3} \lim_{q_0.\vec{q}\to 0} \frac{1}{q_0} \int \frac{d^3k}{(2\pi)^3} \frac{(-\pi)N}{4\omega_k\omega_p} \{C_2\delta(q_0 - \omega_k + \omega_p) \\ &\quad + C_3\delta(q_0 + \omega_k - \omega_p)\} \\ &= \frac{e^2}{3} \lim_{q_0.\vec{q}\to 0} \mathrm{Im}\left[\int \frac{d^3k}{(2\pi)^3} \frac{N}{4\omega_k\omega_p} \lim_{\Gamma\to 0} \right. \\ &\quad \left. \times \left\{ \frac{C_2/q_0}{(q_0 - \omega_k + \omega_p) + i\Gamma} + \frac{C_3/q_0}{(q_0 + \omega_k - \omega_p) + i\Gamma} \right\} \right]. \end{aligned} \tag{17}$$

We take the finite value of Γ in our further calculations to get nondivergent values of σ. In the Kubo approach, this traditional technique is widely used to calculate different transport coefficients like shear viscosity [20,31] and electrical conductivity [19]. In this respect, this formalism is very much close to quasiparticle approximation. The Γ is basically thermal widths of medium constituents, which is physically related with the probabilities of different in-medium scattering. Inverse of Γ measures the relaxation time τ, which is the average time of the medium constituent to reach its equilibrium conditions.

Next, applying the L'Hospital's rule in Eq. (17) (see the Appendix), we get a generalized expression of electrical conductivity for the bosonic (ϕ_π) or fermionic (ψ_N) field,

$$\sigma = \frac{\beta e^2}{3} \int \frac{d^3k}{(2\pi)^3} \frac{(-N^0)}{4\omega_k^2\Gamma} [n_k^-(1 + \epsilon_k n_k^-) + n_k^+(1 + \epsilon_k n_k^+)], \tag{18}$$

where

$$N^0 = \lim_{q_0,\vec{q}\to 0} N(k_0 = \pm\omega_k, \vec{k}, q). \tag{19}$$

Depending upon the sign of ϵ_k, the statistical probability becomes a Bose enhanced ($\epsilon_k = +1$ for bosonic field) or Pauli blocked ($\epsilon_k = -1$ for fermionic field) probability. Following the definition of N^0 in Eq. (19), Eqs. (12) and (13) can be simplified as

$$N^0 = -I_\pi^e(4\vec{k}^2) \quad \text{for } \pi\pi\text{loop}, \tag{20}$$

and

$$N^0 = -I_N^e(8\vec{k}^2) \quad \text{for } NN\text{loop}. \tag{21}$$

Using the above Eqs. (20) and (21) in Eq. (18) as well as their relevant parameters from Eqs. (9) and (10), we get the electrical conductivity of the pionic and nucleonic medium,

$$\sigma_\pi = \frac{\beta e^2}{3} \int_0^\infty \frac{d^3\vec{k}}{(2\pi)^3} \frac{\vec{k}^2}{\omega_k^{\pi 2}\Gamma_\pi} n_k(\omega_k^\pi)\{1 + n_k(\omega_k^\pi)\} \tag{22}$$

and

$$\begin{aligned} \sigma_N = \frac{2\beta e^2}{3} \int_0^\infty \frac{d^3\vec{k}}{(2\pi)^3} \frac{\vec{k}^2}{\omega_k^{N2}\Gamma_N} [n_k^+(\omega_k^N)\{1 - n_k^+(\omega_k^N)\} \\ + n_k^-(\omega_k^N)\{1 - n_k^-(\omega_k^N)\}]. \end{aligned} \tag{23}$$

Hence, adding the pionic and nucleonic components, we get the total electrical conductivity

$$\sigma_T = \sigma_\pi + \sigma_N. \tag{24}$$

This is basically one-loop anatomy of electrical conductivity of hadronic matter, whose higher order issue [32] is addressed in Sec V.

III. THERMAL WIDTH

Let us come to the thermal widths of pion (Γ_π) and nucleon (Γ_N). Pion thermal width can be obtained from the imaginary part of pion self-energy for different mesonic and baryonic loops. Figure 1(b) represents the pion self-energy diagram for πM (mesonic) loops, $\Pi^R_{\pi(\pi M)}$, where $M = \sigma$, ρ mesons, or resonances. Here the subscript in $\Pi^R_{\pi(\pi M)}$ stands for the external (outside the bracket) and

internal (inside the bracket) particles for diagram 1(b). This notation is followed by latter diagrams also. Now, pion self-energy for different baryonic loops ($\Pi^R_{\pi(NB)}$) can have two possible diagrams as shown in Figs. 1(c) and 1(d). Here internal lines NB stand for nucleon (N) and baryon (B), respectively, where different four-star spin $1/2$ and $3/2$ baryons are taken in our calculations. Adding all those mesonic and baryonic loops, we get the total thermal width of pion Γ_π, which can be expressed as

$$\begin{aligned}\Gamma_\pi &= \sum_M \Gamma_{\pi(\pi M)} + \sum_B \Gamma_{\pi(NB)} \\ &= -\sum_M \mathrm{Im}\Pi^R_{\pi(\pi M)}(k_0 = \omega^\pi_k, \vec{k})/m_\pi \\ &\quad - \sum_B \mathrm{Im}\Pi^R_{\pi(NB)}(k_0 = \omega^\pi_k, \vec{k})/m_\pi. \end{aligned} \tag{25}$$

Similarly, nucleon self-energy is shown in Fig. 2(b) and it has been denoted as $\Sigma^R_{N(\pi B)}$, where in the internal lines, we have taken all those spin $1/2$ and $3/2$ baryons (B) as taken in pion self-energy for baryonic loops. Hence, summing all these πB loops, we can express our nucleon thermal width as

$$\Gamma_N = \sum_B \Gamma_{N(\pi B)} = -\sum_B \mathrm{Im}\Sigma^R_{N(\pi B)}(k_0 = \omega^N_k, \vec{k}). \tag{26}$$

Next we discuss briefly the calculations of thermal widths from different one-loop self-energy graphs as shown in Figs. 1 and 2.

A. Pion thermal width for different mesonic loops

To calculate the mesonic loop contribution of pionic thermal width $\Gamma_{\pi(\pi M)}$, the pion self-energy for πM loops has been evaluated and it is expressed as [33]

$$\begin{aligned}\Gamma_{\pi(\pi M)} &= \mathrm{Im}\Pi^R_{\pi(\pi M)}(k_0 = \omega^\pi_k, \vec{k})/m_\pi \\ &= \frac{1}{m_\pi}\int \frac{d^3\vec{l}}{32\pi^2\omega^\pi_l\omega^M_u} \\ &\quad \times L(l_0 = -\omega^\pi_l, \vec{l}, k_0 = \omega^\pi_k, \vec{k})\{n(\omega^\pi_l) \\ &\quad - n(\omega^M_u)\}\delta(\omega^\pi_k + \omega^\pi_l - \omega^M_u), \end{aligned} \tag{27}$$

where $n(\omega^\pi_l)$, $n(\omega^M_u)$ are Bose-Einstein (BE) distribution functions of π, M mesons with energies $\omega^\pi_l = (\vec{l}^2 + m^2_\pi)^{1/2}$ and $\omega^M_u = (|\vec{k} - \vec{l}|^2 + m^2_M)^{1/2}$, respectively. The vertex factors $L(k, l)$ [33] have been obtained from the effective Lagrangian density,

$$\mathcal{L} = g_\rho \vec{\rho}_\mu \cdot \vec{\pi} \times \partial^\mu \vec{\pi} + \frac{g_\sigma}{2} m_\sigma \vec{\pi} \cdot \vec{\pi}\sigma. \tag{28}$$

B. Pion thermal width for different baryonic loops

Along with the mesonic loops, different baryon loops may provide some contributions in pion thermal width. This component can be derived from pion self-energy for different NB loops, where $B = N(940)$, $\Delta(1232)$, $N^*(1440)$, $N^*(1520)$, $N^*(1535)$, $\Delta^*(1600)$, $\Delta^*(1620)$, $N^*(1650)$, $\Delta^*(1700)$, $N^*(1700)$, $N^*(1710)$, $N^*(1720)$ are taken [34,35]. The masses of all the four-star baryon resonances (in MeV) are presented inside the brackets. The direct and cross diagrams of pion self-energy for NB loops are shown in Figs. 1(c) and 1(d). Adding the relevant Landau cut contributions of both diagrams (c) and (d), the total thermal width of the pion for any NB loop is given by [34,35]

$$\begin{aligned}\Gamma_{\pi(NB)} &= \mathrm{Im}\Pi^R_{\pi(NB)}(k_0 = \omega^\pi_k, \vec{k})/m_\pi \\ &= \frac{1}{m_\pi}\int \frac{d^3\vec{l}}{32\pi^2\omega^N_l\omega^B_u} \\ &\quad \times [L(l_0 = \omega^N_l, \vec{l}, k_0 = \omega^\pi_k, \vec{k})\{n^+_l(\omega^N_l) \\ &\quad - n^+_u(\omega^B_u)\}\delta(\omega^\pi_k - \omega^N_l + \omega^B_u) \\ &\quad + L(l_0 = -\omega^N_l, \vec{l}, k_0 = \omega^\pi_k, \vec{k})\{-n^-_l(\omega^N_l) \\ &\quad + n^-_u(\omega^B_u)\}\delta(\omega^\pi_k + \omega^N_l - \omega^B_u)], \end{aligned} \tag{29}$$

where $n^\pm(\omega^N_l)$, $n^\pm(\omega^B_u)$ are Fermi-Dirac (FD) distribution functions of N, B ($\pm$ for particle and antiparticle) with energies $\omega^N_l = (\vec{l}^2 + m^2_N)^{1/2}$ and $\omega^B_u = (|\pm\vec{k} + \vec{l}|^2 + m^2_B)^{1/2}$ ($\pm$ for two different diagrams), respectively. With the help of the effective Lagrangian densities [36],

$$\begin{aligned}\mathcal{L} &= \frac{f}{m_\pi}\overline{\psi}_B\gamma^\mu \begin{Bmatrix} i\gamma^5 \\ \mathbb{1} \end{Bmatrix}\psi_N\partial_\mu\pi + \mathrm{H.c.} \quad \text{for } J^P_B = \frac{1^\pm}{2}, \\ \mathcal{L} &= \frac{f}{m_\pi}\overline{\psi}^\mu_B \begin{Bmatrix} \mathbb{1} \\ i\gamma^5 \end{Bmatrix}\psi_N\partial_\mu\pi + \mathrm{H.c.} \quad \text{for } J^P_B = \frac{3^\pm}{2}, \end{aligned} \tag{30}$$

the vertex factors $L(k, l)$ [34,35] have been found.

C. Nucleon thermal width

The nucleonic thermal width has been calculated from nucleon self-energy for different possible πB loops, where B stands for all the baryons as taken in pion self-energy for baryonic loops. Evaluating the loop diagram, shown in Fig. 2(b), we get [37,38]

$$\begin{aligned}\Gamma_{N(\pi B)} &= -\mathrm{Im}\Sigma^R_{N(\pi B)}(k_0 = \omega^N_k, \vec{k}) \\ &= \int \frac{d^3\vec{l}}{32\pi^2\omega^\pi_l\omega^B_u} \\ &\quad \times L(l_0 = -\omega^\pi_l, \vec{l}, k_0 = \omega^N_k, \vec{k})\{n(\omega^\pi_l) \\ &\quad + n^+(\omega^B_u)\}\delta(\omega^N_k + \omega^\pi_l - \omega^B_u), \end{aligned} \tag{31}$$

where $n(\omega_l^\pi)$ and $n^+(\omega_u^B)$ are BE and FD distribution functions for π and B with energies $\omega_l^\pi = (\vec{l}^2 + m_\pi^2)^{1/2}$ and $\omega_u^B = (|\vec{k} - \vec{l}|^2 + m_B^2)^{1/2}$, respectively.

The vertex factors $L(k, l)$ [37,38] have been deduced by using the πNB interaction Lagrangian densities from Eq. (30).

IV. RESULTS AND DISCUSSION

Equations (25), (27), and (29) are able to estimate the thermal width of the pion, whose off-shell and on-shell values are elaborately discussed in Refs. [33–35]. Similarly, the off-shell and on-shell properties of the nucleon thermal width are addressed in Refs. [37–39]. The results of the pion in Ref. [34] and nucleon in Ref. [39] are compared with some of the earlier estimations and they are more or less compatible with each other. Although, some differences in their numerical strengths are noticed because of their pictorial and methodological differences.

Using the $\Gamma_{\pi(\pi\sigma)}(\vec{k}, T)$, $\Gamma_{\pi(\pi\rho)}(k, T)$ and their total in the integrand of Eq. (22), the dotted, dashed, and solid lines of Fig. 3 are generated, where folding [33] by vacuum spectral functions of resonances σ and ρ is considered in panel (a) but not in panel (b). Like the results of shear viscosity in the earlier work [33], σ and ρ resonances play a dominant role in the electrical conductivity for being nondivergent and finite at low ($T < 0.100$ GeV) and high ($T > 0.100$ GeV) temperature domain, respectively. This is because the thermal widths of $\pi\sigma$ and $\pi\rho$ loops have dominant values in the low and high T domain, respectively. We get $\sigma_\pi(T)$ as a decreasing function in low and high temperature both, although a mild increasing function of shear viscosity $\eta_\pi(T)$ has been observed in Ref. [33] at the high temperature domain of hadronic matter (0.100 GeV $< T < 0.175$ GeV).

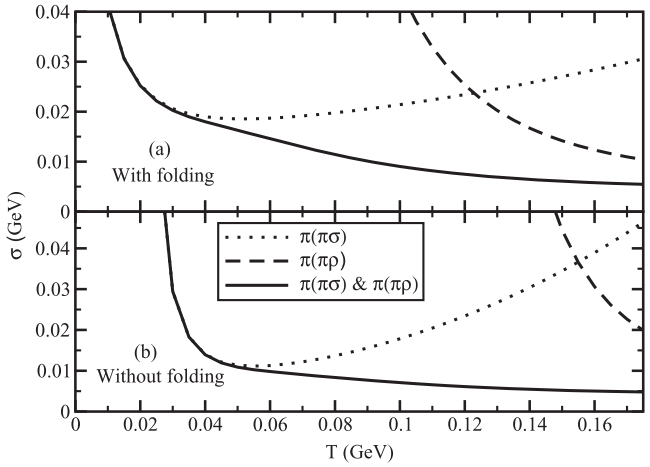

FIG. 3. Temperature dependence of electrical conductivity for the pionic medium due to its different mesonic loops, $\pi\sigma$ (dotted line), $\pi\rho$ (dashed line) loops and their total (solid line). With and without the folding effect of resonances $M = \sigma, \rho$ are taken in the upper (a) and lower (b) panels, respectively.

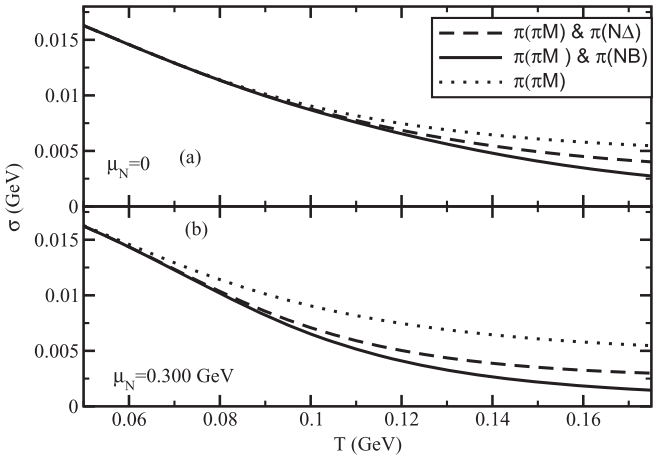

FIG. 4. Effect of baryonic loops ($N\Delta$ loop, dashed line; NB loops, solid line) after adding with mesonic loops (πM loops, dotted line) of the pion on $\sigma_\pi(T)$ at $\mu_N = 0$ (a) and $\mu_N = 0.300$ GeV (b).

The mathematical origin for these differences in the nature of $\sigma_\pi(T)$ and $\eta_\pi(T)$ is the different power of momentum ($\vec{k}^4$ for σ_π but $\vec{k}^6$ for η_π) in the numerator of their respective integrands.

Adding baryonic loop contributions with the mesonic loops of pion self-energy, we get the total thermal width of the pion as described explicitly in Eq. (25). Figures 4(a) and 4(b) for $\mu_N = 0$ and 0.300 GeV reveal that $\sigma_\pi(T)$ reduces after adding baryonic loop contribution in pion self-energy and its reduction strength becomes larger for larger values of μ_N as baryonic loop contribution, $\Gamma_{\pi(NB)}(\vec{k}, T, \mu_N)$, depends sensitively on μ_N. To display the dominant contribution of the $N\Delta$ loop [$\Gamma_{\pi(N\Delta)}$], Fig. 4 shows individual contributions of meson loops, meson loops + $N\Delta$ loop, and meson + baryon loops by dotted, dashed, and solid lines, respectively.

Next, Figs. 5(a) and 5(b) for $T = 0.120$ and 0.150 GeV show μ_N dependence of electrical conductivity of the pionic component for meson loops (dotted line), meson loops + $N\Delta$ loop (dashed line), and meson + baryon loops (solid line). As $\Gamma_{\pi(\pi M)}(\vec{k}, T)$ is independent of μ_N, the corresponding σ_π (dotted line) remain constant with the variation of μ_N. After adding the $N\Delta$ loop (dashed line) and other baryon loops (solid line), a decreasing nature of $\sigma_\pi(\mu_N)$ is clearly noticed. A sensitive dependence of μ_N in $\Gamma_{\pi(NB)}$ for the $N\Delta$ loop (dominant) and other baryon loops is the main reason behind the decreasing nature of $\sigma_\pi(\mu_N)$. The reader should keep in mind that addition of different loops in Figs. 3–5 occurred in pion thermal width, guided by Eq. (25), but not in conductivity.

In Figs. 6(a) and 6(b) for $\mu_N = 0.500$ and 0.300 GeV, the T dependence of pionic (σ_π) and nucleonic (σ_N) components of electrical conductivities and their total (σ_T) are shown by dotted, dashed, and solid lines, respectively.

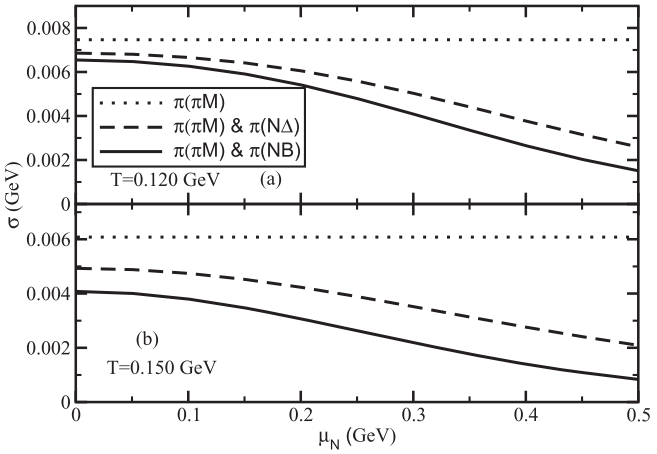

FIG. 5. The same as Fig. 4 for $\sigma_\pi(\mu_N)$ at $T = 0.120$ (a) and $T = 0.150$ GeV (b).

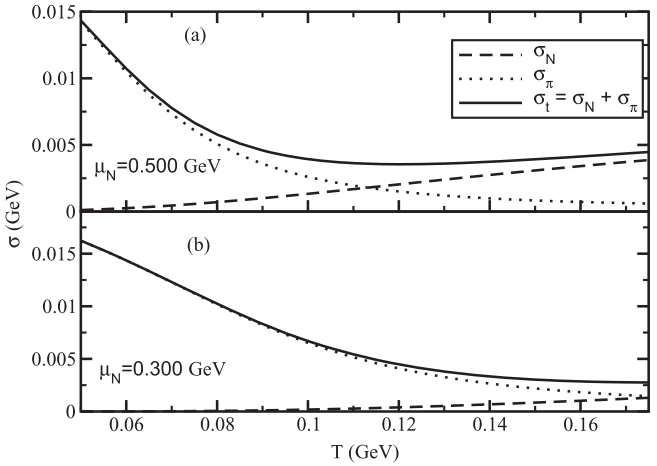

FIG. 6. Temperature dependence of electrical conductivity for pion (dotted line) and nucleon (dashed line) components and their total (solid line) at $\mu_N = 0.500$ (a) and $\mu_N = 0.300$ GeV.

Corresponding results in the μ_N axis are shown in Figs. 7(a) and 7(b) for $T = 0.120$ and 0.150 GeV. Unlike the σ_π, the σ_N increases with both T and μ_N. The T, μ_N dependence in the expression of conductivity is basically coming from the phase space factor and thermal width of the medium constituents. The nucleon phase space factor (statistical weight factor, built by FD distributions) is more dominating than its thermal width $\Gamma_N(T, \mu_N)$ in controlling T, μ_N dependences of σ_N. Whereas, for the pionic case, $\Gamma_\pi(T, \mu_N)$ becomes more influential than the pionic phase factor (statistical Bose enhanced weight factor). This is the mathematical reason for the opposite nature of $\sigma_\pi(T, \mu_N)$ and $\sigma_N(T, \mu_N)$. From a simultaneous observation of Figs. 6 and 7, we can conclude that the decreasing nature of $\sigma_T(T, \mu_N)$ becomes inverse beyond certain points of T and μ_N, where σ_T exposes the points of minima. This behavior can be visualized well from Fig. 8, which exhibits a three-dimensional plot of $\sigma_T(T, \mu_N)$.

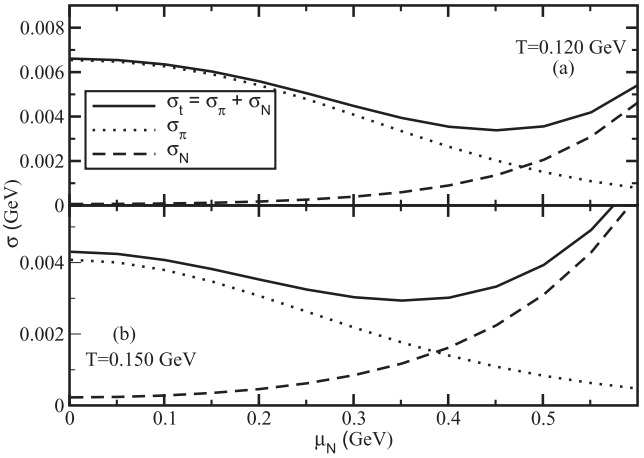

FIG. 7. μ_N dependence of electrical conductivity for pion (dotted line) and nucleon (dashed line) components and their total (solid line) at $T = 0.120$ (a) and $T = 0.150$ GeV.

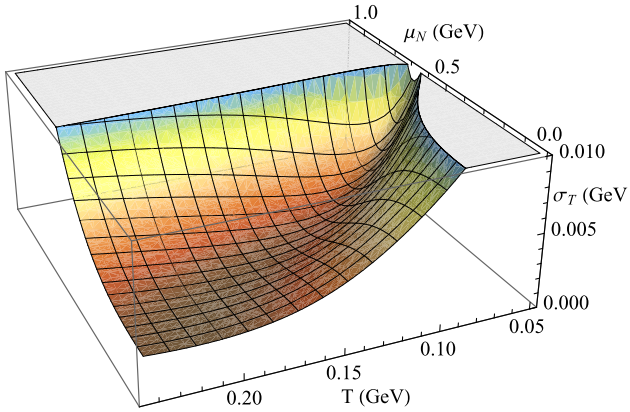

FIG. 8. Total electrical conductivity σ_T in the $T - \mu_N$ plane.

Up to now, our results are presented by taking $e^2 = 1$. After multiplying by $e^2 = 4\pi/137$, exact values of σ_T have been shown in the last two figures 9 and 10. Figure 9(a) displays a comparison of present results with the earlier results, obtained by Fraile *et al.* [20] (stars and triangles), Lee *et al.* [18] (open circles), Marty *et al.* [12] (squares), and Cassing *et al.* [11] (solid circles) at hadronic temperature domain for $\mu_N = 0$. Within $0.110\ \text{GeV} < T < 0.175$ GeV, present results more or less agree with the results of Ref. [18,20] but are substantially smaller than the results of Ref. [11,12]. Figure 9(b) shows σ_T vs T at three different values of μ_N, where we notice the shifting of minimum values of σ_T towards lower T as one increases μ_N. Alternatively, these minimum values of σ_T are also shifted towards lower μ_N as T increases, which is explicitly shown in Fig. 10(a). Next, Fig. 10(b) represents the points of minima for σ_T in the $T - \mu_N$ plane. An approximated freeze-out line (solid line), taken from Ref. [40], is also added in Fig. 10(b). The points of minima, which are located outside the freeze-out line, can only be covered by

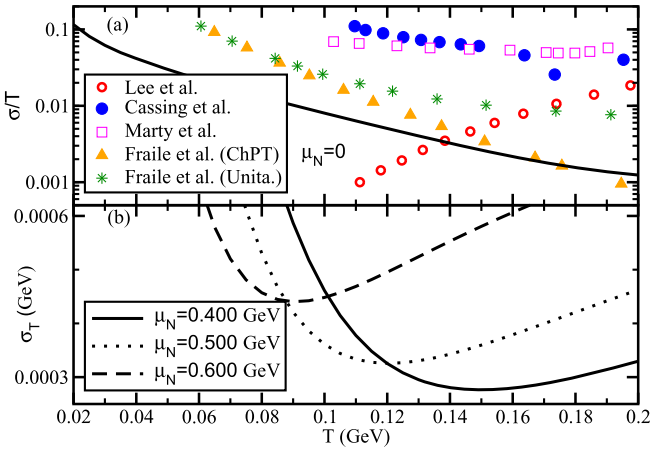

FIG. 9. Our results of $\sigma(T,\mu_N=0)/T$ are compared with the results of Refs. [11,12,18,19] (a). The valley structure of $\sigma(T)$ at $\mu_N=0.400$, 0.500, and 0.600 GeV is shown by solid, dotted, and dashed lines, respectively, in panel (b).

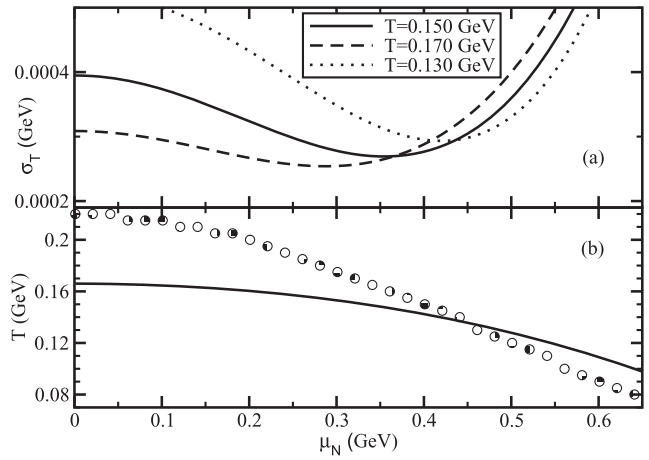

FIG. 10. (a) Valley structure of $\sigma(\mu_N)$ at three different T. (b) The points of minima (solid circles) and the freeze-out line [40] (solid line) are shown in the $T-\mu_N$ plane.

the expanding fireball, produced in different beam energies of heavy ion collisions. Therefore, the minima or valley structure can be observed from ($T_f\approx 0.166$ GeV, $\mu_f\approx 0$) to ($T_f\approx 0.140$ GeV, $\mu_f\approx 0.420$ GeV), where subscript f stands for freeze-out. In other words, this valley structure may be observed from higher beam energy $\sqrt{s}=200$ GeV to lower beam energy $\sqrt{s}\approx 8$ GeV. However, this issue may be confirmed after further research on σ-calculations at finite baryon density, based on a different effective QCD model.

We have presented the numerical values of $\sigma(T,\mu_N=0)/T$, estimated by earlier works in Table I, where most of the works display the decreasing $\sigma(T)/T$ in hadronic temperature [11,12,19,20] and increasing $\sigma(T)/T$ in the temperature domain of the quark phase [11–17,28]. Among them, Refs. [11,12], covering both temperature domains, have found the minimum value of σ/T near the transition temperature. The exact quantitative comparison of different values of $\sigma(T)/T$ may not be so meaningful as the methods or models of different studies are very diverse. In that respect, the reader may have to take a rough view on the table just for being updated with numerical strength and nature of $\sigma(T)/T$, obtained from different investigations.

The present methodology for calculation of electrical conductivity can be applicable to estimate dilepton and photon production from hadronic matter. The σ is basically the static limit estimation of the electromagnetic current-current correlator, whose dynamical structure is directly related with the dilepton rate. Hence, the future plan of the present work is to focus on the detail structure of the correlator in the energy and momentum plane instead of its limiting value at the origin. In this context, we should keep in mind that in-medium modification of the ρ meson via the vector dominance model (VDM) plays the dominating role in the thermal dilepton rate from hadronic matter [1,2]. However, it does not have any contribution in σ, because the ρ-spectral function at zero energy and momentum becomes 0. So, the dynamical structure of σ, based on the current methodology, may have to be added to the traditional VDM calculation of the thermal dilepton rate. Following Refs. [19,20], one can estimate the thermal photon production rate from hadronic matter at zero momentum. The present methodology of σ calculation may have some important phenomenological impact on this dilepton and photon production, which can be investigated in future by revisiting the earlier works [2,41,42], related with these electromagnetic probes.

V. HIGHER ORDER ISSUE

The diagrammatic calculations of the transport coefficient via Kubo formalism always suffer from the issue of higher order contributions [32]. For our present interaction picture, the issue is as follows. Let us take one-loop expression of the pionic medium, given in Eq. (22), which has an order $\mathcal{O}(\frac{1}{\Gamma_\pi})\sim\mathcal{O}(\frac{1}{g^2_{\sigma\pi\pi}})$, as $\Gamma_\pi\sim g^2_{\sigma\pi\pi}$, when we deal with the $\sigma\pi\pi$ interaction only. After this one-loop diagram, as shown in Fig. 1(a), the two point function of Eq. (1) or (2) can have two-loop-type anatomy, where an additional internal line of the σ meson is drawn from upper to lower internal lines of pions in Fig. 1(a). Interestingly, this two-loop diagram also has the same order as the one-loop diagram because the extra $1/\Gamma_\pi$ from the second loop of this two-loop diagram is canceled by its additional vertex factor $g^2_{\sigma\pi\pi}$ and hence, its net order is $\mathcal{O}(\frac{1}{\Gamma_\pi}g^2_{\sigma\pi\pi}\frac{1}{\Gamma_\pi})\sim\mathcal{O}(\frac{1}{\Gamma_\pi})\sim\mathcal{O}(\frac{1}{g^2_{\sigma\pi\pi}})$. Not only this two loop but all of the higher order ladder diagrams may have this same order. However, for this present interaction picture, the numerical strength in transport coefficient for the two-loop diagram appears to be lower than that for the one-loop diagram. This has been found for the shear viscosity calculation in

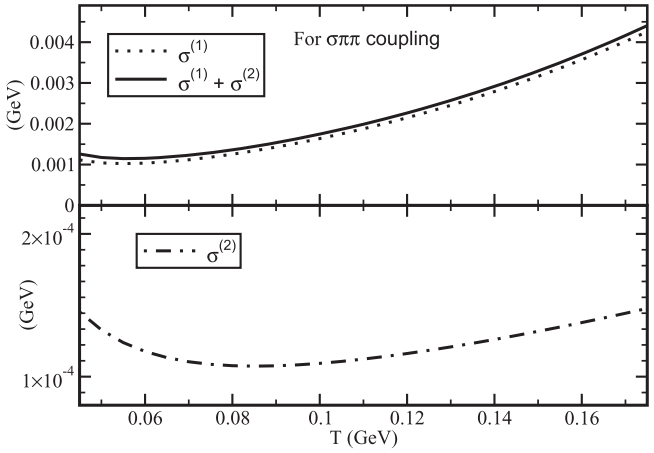

FIG. 11. One-loop and two-loop contributions of electrical conductivity of pionic medium for $\sigma\pi\pi$ interaction are shown by the dotted line (a) and dash-dotted line (b). The solid line (a) is their total.

Ref. [31], where some specific $\phi\phi\Phi$-type interaction (with $m_\Phi > m_\phi$) has been considered. Following a similar calculation for electrical conductivity like shear viscosity in Ref. [31], the two-loop contribution $\sigma^{(2)}$ has been obtained and compared with one-loop values, $\sigma^{(1)}$, as shown in Fig. 11. We notice in Fig. 11 that two-loop contribution (dash-dotted line) may safely be ignored with respect to the numerical strength of the one-loop diagram (dotted line) and one-loop contribution may be considered as a rough (or maybe leading) estimation instead of the total (solid line). The thermal distribution function of high mass resonance like the σ meson may be a major reason for suppressing $\sigma^{(2)}$, as also observed for shear viscosity in Ref. [31]. On the basis of this fact, we may also ignore higher order loop diagrams, which contain a higher number of high mass resonances in the internal lines.

Again, the thermal width pion or nucleon may also come from two-loop or higher order loop diagrams besides the one-loop diagram, shown in Figs. 1(b)–1(d) and 2(b). In this context, our methodology, based on the phenomenological hadronic model, may not be treated equivalently with the perturbative calculations like Chiral perturbation theory. Since the coupling constants are tuned from the experimental decay widths of high mass resonances (e.g., σ, ρ, Δ, etc.), the one-loop contribution gives more phenomenological interaction strength than the higher order loop diagrams.

A final remark is in order that the present estimation of electrical conductivity of the pionic and nucleonic medium is based on the one-loop skeleton of its current-current correlator as well as its thermal widths being also calculated from one-loop self-energies of the pion and nucleon. This present methodology can be understood as follows. Starting from electromagnetic current-current correlators of the pion and nucleon with the help of their free Lagrangian densities, we get one-loop anatomy of the correlators, which are basically diverged. Then, the finite thermal widths of internal lines in the one-loop diagrams have to be considered for getting nondivergent and finite values of electrical conductivities of pionic and nucleonic components. In this way, a quasiparticle scenario is introduced in the diagrammatic calculation of the Kubo framework. We may impose the entire interaction picture in this quantity—thermal width—because this quantity basically makes the picture of free theory transform into the interaction picture. So thermal width may have to estimate from interaction Lagrangian density, while the structure of the transport coefficient like electrical conductivity may have to estimate from free Lagrangian density. Being exactly equivalent with the method of relaxation time approximation, this methodology may be considered a more acceptable and economic methodology. An alternative first possible way is to start with the total Lagrangian density and consider all possible higher order loop diagrams, which will be diverged individually like one-loop if we do not impose any thermal width in the internal lines of the diagrams. It implies that introducing the quasiparticle picture is very essential to cure divergence in transport coefficient calculation. Now, the second possible alternative method is to consider all higher order loop diagrams with finite thermal width. In this case, though, we can grossly understand that the higher order loop may have the same order as one loop as the additional vertex factor is eventually canceled by the couplings of the additional thermal width in the higher order loop diagram. However, in realistic numerical estimation, the scenario may be different because of additional thermal structure of the diagram. As an example, in this present analysis for $\sigma\pi\pi$ interaction, we notice that two-loop contribution is suppressed because of the thermal structure of the σ meson internal line. Hence, higher order loop diagrams, containing more σ meson internal lines, are more suppressing. The complexity arises during the two-loop calculations for other interactions like $\rho\pi\pi$, $BN\pi$ interaction, whose vertex factors contain momentum dependent structure. However, owing to the same logic, we may conclude that they are also suppressed like the $\sigma\pi\pi$ interaction because of the thermal structure of the ρ meson and baryons B.

VI. SUMMARY AND CONCLUSION

The present work has provided an estimation of electrical conductivity of hadronic medium at finite temperature and baryon density. Assuming the pion and nucleon are the most abundant medium constituents, we have first deduced thermal correlators of their electromagnetic currents and then, taking the static limits of these correlators, the expressions of electrical conductivities for pionic and nucleonic components are derived. To get the nondivergent values of these correlators in their static limits, one has to include the finite thermal widths of the medium constituents—the pion and nucleon. This is a traditional quasiparticle technique of the Kubo framework, used during the calculations of transport coefficients from the relevant correlators in their static limits. Following the field

theoretical version of the optical theorem, the thermal widths of the pion and nucleon are obtained from the imaginary part of their one-loop self-energy diagrams, which accommodate different mesonic and baryonic resonances in the intermediate states. As a dynamical part, the interactions of the pion and nucleon with other mesonic and baryonic resonances are guided by the effective hadronic Lagrangian densities, where their couplings are tuned by the decay width of resonances, based on the experimental data from PDG. The momentum distribution of these thermal widths are integrated out during evaluation of electrical conductivities of respective components.

The electrical conductivity for the pionic component is obtained as a decreasing function T and μ_N, where mesonic loops are dominant to fix its numerical strength. The $\pi\sigma$ and $\pi\rho$ loops of pion self-energy control the strength of electrical conductivity at low and high T regions, respectively, while a further reduction of numerical values in conductivity at high T domain is noticed after the addition of different baryonic loops in the pion self-energy. Electrical conductivity of the pionic component due to mesonic loops remains constant with μ_N but it is transformed to a decreasing function when the baryonic loops are added in the pion self-energy. The nucleonic component gives the increasing values of electrical conductivity with the variation of T and μ_N. After adding these pionic and nucleonic components, the total electrical conductivity first decreases at the pion dominating $T-\mu_N$ domain and then increases at the nucleonic dominating domain. Therefore, the numerical results show a set of $T-\mu_N$ points, where total electrical conductivity becomes minimum.

Comparing with earlier estimations of electrical conductivity at $\mu_N=0$, present work more or less agrees with Refs. [18,20] quantitatively. We are also noticing that the present work is qualitatively similar with most of the earlier works [11,12,19–21], which show that electrical conductivity at $\mu_N=0$ decreases with T.

The present work has considered the pion and nucleon as abundant medium constituents, made of u and d quarks. However, the K meson and Λ baryon may have to be considered when we extend our calculation to the strange sector, which is in under progress and planned to zoom in on the strange sector effect elaborately in a future article.

ACKNOWLEDGMENTS

This work is financially supported by the UGC Dr. D. S. Kothari Postdoctoral Fellowship under Grant No. F.4-2/2006 (BSR)/PH/15-16/0060.

APPENDIX: SOME DETAIL PART OF CONDUCTIVITY CALCULATION

1. Calculation $N(\vec{q},\vec{k})$

Let us write the 11 component of the two point function of the current-current correlator in terms of field operators. For the ϕ_π field it is given by

$$\Pi_{11}(q) = i\int d^4x e^{iqx}\langle TJ^{\rm EM}_\mu(x)J^\mu_{\rm EM}(0)\rangle_\beta = ie^2\int d^4x e^{iqx}\langle T\phi_\pi(x)\partial_\mu\phi_\pi(x)\phi_\pi(0)\partial^\mu\phi_\pi(0)\rangle_\beta. \tag{A1}$$

With the help of the Wick's contraction technique, we have

$$\Pi_{11}(q) = ie^2\int d^4x e^{iqx}[\langle T\phi_\pi\underbrace{(x)\partial_\mu\phi_\pi\overbrace{(x)\phi_\pi}(0)\partial^\mu\phi_\pi}(0)\rangle_\beta = ie^2\int\frac{d^4k}{(2\pi)^4}N(q,k)D_{11}(k)D_{11}(p=q-k), \tag{A2}$$

where

$$N(q,k) = (-4)k^\mu(q-k)_\mu \tag{A3}$$

and its space component part is

$$N(\vec{q},\vec{k}) = (-4)\{-\vec{k}\cdot\vec{q}+\vec{k}^2\}. \tag{A4}$$

Similarly for the ψ_N field,

$$\Pi_{11}(q) = ie^2\int d^4x e^{iqx}\langle T\overline{\psi}_N\underbrace{(x)\gamma_\mu\psi_N\overbrace{(x)\overline{\psi}_N}(0)\gamma^\mu\psi_N}(0)\rangle_\beta = ie^2\int\frac{d^4k}{(2\pi)^4}N(q,k)D_{11}(k)D_{11}(p=q+k), \tag{A5}$$

where

$$N(q,k) = {\rm Tr}[\gamma^\mu(q\!\!/+k\!\!/+m_\psi)\gamma_\mu(k\!\!/+m_\psi)] = 8k^\mu(q+k)_\mu - 4[k\cdot(q+k)-m_\psi^2]g^\mu_\mu \tag{A6}$$

and the space component part of

$$N(q,k_0=\pm\omega_k,\vec{k}) = 8k^\mu(q+k)_\mu - 4[k\cdot q]g^\mu_\mu \tag{A7}$$

is

$$N(\vec{q},\vec{k}) = -8\vec{k}\cdot(\vec{q}+\vec{k})+4[\vec{k}\cdot\vec{q}]g^i_i. \tag{A8}$$

2. Application of L'Hospital rule

For finite value of Γ, Eq. (17) becomes

$$\sigma = \frac{e^2}{3}\int\frac{d^3k}{(2\pi)^3}\frac{N^0}{4\omega_k^2\Gamma}\lim_{q_0,\vec{q}\to0}\left[\frac{C_2}{q_0}+\frac{C_3}{q_0}\right], \tag{A9}$$

as

$$\lim_{\vec{q}\to0}\omega_p = \omega_k. \tag{A10}$$

Applying L'Hospital's rule, we can write

$$\lim_{q_0\to 0}\frac{C_{2,3}(q_0)}{q_0} = \lim_{q_0\to 0}\frac{\frac{d}{dq_0}\{C_{2,3}(q_0)\}}{\frac{d}{dq_0}\{q_0\}} = \frac{d}{dq_0}\{\pm n_p^{\mp}(\omega_p = \mp\, q_0+\omega_k)\} = \beta[n_k^{\mp}(1+\epsilon_k n_k^{\mp})], \tag{A11}$$

since

$$(\pm)\frac{d}{dq_0}n_p^{\mp}(\omega_p = \mp\, q_0+\omega_k) = (\pm)\frac{-\beta\frac{d\omega_p}{dq_0}e^{\beta(\omega_p\pm\mu)}}{\{e^{\beta(\omega_p\pm\mu)}+\epsilon_k\}^2}$$

$$\lim_{q_0\to 0}(\pm)\frac{d}{dq_0}n_p^{\mp}(\omega_p = \mp\, q_0+\omega_k) = (\pm)\frac{-\beta(\mp)e^{\beta(\omega_k\pm\mu)}}{\{e^{\beta(\omega_k\pm\mu)}+\epsilon_k\}^2} = \beta[n_k^{\mp}(1+\epsilon_k n_k^{\mp})]. \tag{A12}$$

[1] R. Rapp, Adv. High Energy Phys. **2013**, 1 (2013); R. Rapp and J. Wambach, Adv. Nucl. Phys. **25**, 148253 (2000).
[2] P. Mohanty, S. Ghosh, and S. Mitra, Adv. High Energy Phys. **2013**, 176578 (2013).
[3] R. Arnaldi *et al.* (NA60 Collaboration), Phys. Rev. Lett. **100**, 022302 (2008); **61**, 711 (2009); S. Damjanovic *et al.* (NA60 Collaboration), J. Phys. G **35**, 104036 (2008).
[4] E. Braaten and R. D. Pisarski, Nucl. Phys. **B337**, 569 (1990).
[5] C. A. Islam, S. Majumder, N. Haque, and M. G. Mustafa, J. High Energy Phys. 02 (**2015**) 011.
[6] A. Bzdak and V. Skokov, Phys. Lett. B **710**, 171 (2012).
[7] K. Tuchin, Adv. High Energy Phys. **2013**, 490495 (2013).
[8] Y. Akamatsu, H. Hamagaki, T. Hatsuda, and T Hirano, J. Phys. G **38**, 124184 (2011).
[9] Y. Yin, Phys. Rev. C **90**, 044903 (2014).
[10] Y. Hirono, M. Hongo, and T. Hirano, Phys. Rev. C **90**, 021903 (2014).
[11] W. Cassing, O. Linnyk, T. Steinert, and V. Ozvenchuk, Phys. Rev. Lett. **110**, 182301 (2013).
[12] R. Marty, E. Bratkovskaya, W. Cassing, J. Aichelin, and H. Berrehrah, Phys. Rev. C **88**, 045204 (2013).
[13] A. Puglisi, S. Plumari, and V. Greco, Phys. Rev. D **90**, 114009 (2014); J. Phys. Conf. Ser. **612**, 012057 (2015); Phys. Lett. B **751**, 326 (2015).
[14] M. Greif, I. Bouras, Z. Xu, and C. Greiner, Phys. Rev. D **90**, 094014 (2014); J. Phys. Conf. Ser. **612**, 012056 (2015).
[15] P. K. Srivastava, L. Thakur, and B. K. Patra, Phys. Rev. C **91**, 044903 (2015).
[16] S. I. Finazzo and J. Noronha, Phys. Rev. D **89**, 106008 (2014).
[17] S. Mitra and V. Chandra, Phys. Rev. D **94**, 034025 (2016).
[18] C. Lee and I. Zahed, Phys. Rev. C **90**, 025204 (2014).
[19] D. Fernandez-Fraile and A. Gomez Nicola, Phys. Rev. D **73**, 045025 (2006).
[20] D. Fernandez-Fraile and A. Gomez Nicola, Eur. Phys. J. C **62**, 37 (2009).
[21] M. Greif, C. Greiner, and G. S. Denicol, Phys. Rev. D **93**, 096012 (2016).
[22] H. T. Ding, A. Francis, O. Kaczmarek, F. Karsch, E. Laermann, and W. Soeldner, Phys. Rev. D **83**, 034504 (2011).
[23] G. Aarts, C. Allton, J. Foley, S. Hands, and S. Kim, Phys. Rev. Lett. **99**, 022002 (2007).
[24] P. V. Buividovich, M. N. Chernodub, D. E. Kharzeev, T. Kalaydzhyan, E. V. Luschevskaya, and M. I. Polikarpov, Phys. Rev. Lett. **105**, 132001 (2010).
[25] Y. Burnier and M. Laine, Eur. Phys. J. C **72**, 1902 (2012).
[26] S. Gupta, Phys. Lett. B **597**, 57 (2004).
[27] B. B. Brandt, A. Francis, H. B. Meyer, and H. Wittig, J. High Energy Phys. 03 (**2013**) 100.
[28] A. Amato, G. Aarts, C. Allton, P. Giudice, S. Hands, and J. I. Skullerud, Phys. Rev. Lett. **111**, 172001 (2013).
[29] D. N. Zubarev, *Nonequilibrium Statistical Thermodynamics* (Consultants Bureau, New York, 1974).
[30] R. Kubo, J. Phys. Soc. Jpn. **12**, 570 (1957).
[31] S. Ghosh, Int. J. Mod. Phys. A **29**, 1450054 (2014).
[32] S. Jeon, Phys. Rev. D **52**, 3591 (1995).
[33] S. Ghosh, G. Krein, and S. Sarkar, Phys. Rev. C **89**, 045201 (2014).
[34] S. Ghosh, J. Phys. G **41**, 095102 (2014).
[35] S. Ghosh, Braz. J. Phys. **45**, 687 (2015).
[36] M. Post, S. Leupold, and U. Mosel, Nucl. Phys. **A741**, 81 (2004).
[37] S. Ghosh, Phys. Rev. C **90**, 025202 (2014).
[38] S. Ghosh, Braz. J. Phys. **44**, 789 (2014).
[39] S. Ghosh, S. Sarkar, and S. Mallik, Phys. Rev. C **82**, 045202 (2010).
[40] F. Karsch and K. Redlich, Phys. Lett. B **695**, 136 (2011).
[41] S. Ghosh, S. Sarkar, and J. Alam, Eur. Phys. J. C **71**, 1760 (2011); S. Sarkar and S. Ghosh, J. Phys. Conf. Ser. **374**, 012010 (2012).
[42] P. Mohanty, V. Roy, S. Ghosh, S. K. Das, B. Mohanty, S. Sarkar, J. Alam, and A. K. Chaudhuri, Phys. Rev. C **85**, 031903 (2012).